Construction and Building Materials 298 (2021) 123862

Contents lists available at ScienceDirect

Construction and Building Materials

journal homepage: www.elsevier.com/locate/conbuildmat

# Experimental research on salt contamination procedures and methods for assessment of the salt distribution

Cristiana Nunes [a,*], Asel Maria Aguilar Sanchez [b], Sebastiaan Godts [c], Davide Gulotta [d], Ioannis Ioannou [e], Barbara Lubelli [f], Beatriz Menendez [g], Noushine Shahidzadeh [h], Zuzana Slížková [a], Magdalini Theodoridou [i]

[a] Institute of Theoretical and Applied Mechanics of the Czech Academy of Sciences, Prosecká 76, 190 00 Prague, Czech Republic
[b] ETH Zürich, Institut für Baustoffe (IfB), Physical Chemistry of Building Materials, Stefano-Franscini-Platz 3, 8093 Zurich, Switzerland
[c] Royal Institute for Cultural Heritage (KIK-IRPA), Jubelpark 1, 1000 Brussels, Belgium
[d] Getty Conservation Institute, 1200 Getty Center Drive, Los Angeles, CA 90049, USA
[e] University of Cyprus, 1 University Avenue, 2109 Aglantzia, Cyprus
[f] Delft University of Technology, Faculty of Architecture, Julianalaan 134, 2628 BL, Delft, the Netherlands
[g] CY Cergy Paris University, Geosciences and Environment Cergy, 1 rue Descartes, 95000 Neuville sur Oise, France
[h] University of Amsterdam, Institute of Physics, Science Park 904-1098XH Amsterdam, the Netherlands
[i] Newcastle University, Hub for Biotechnology in the Built Environment, Devonshire Building, NE1 7RU, Newcastle upon Tyne, United Kingdom

## HIGHLIGHTS

- A procedure for accumulating salts at the surface of porous materials is proposed.
- Most of the salt is concentrated in the first millimetres of the subsurface.
- The measurement of the salt distribution is crucial in salt crystallisation tests.

## ARTICLE INFO

*Article history:*
Received 21 December 2020
Received in revised form 1 June 2021
Accepted 3 June 2021

*Keywords:*
Salt crystallisation test
Porous materials
Salt accumulation
Salt distribution

## ABSTRACT

The RILEM TC ASC-271 is developing a new laboratory test to assess the durability of porous building materials to salt crystallisation. The test encompasses two phases: salt accumulation and damage propagation. This paper focuses on designing a procedure for the accumulation phase; this is considered successful when salts crystallise at the material's evaporative surface (common situation observed on site) without the occurrence of damage. Two procedures were developed and tested on two limestones with different porosity: (1) capillary absorption of a salt solution followed by drying, and (2) continuous capillary absorption. Sodium chloride or sodium sulphate solutions were used. Several methods for assessing the salt distribution were employed: ultrasonic pulse velocity, drilling/scratching resistance, hygroscopic moisture content, ion chromatography, scanning electron microscopy, and micro X-ray fluorescence. The results enabled the selection of the most effective protocol for the salt accumulation phase.


## 1. Introduction

Salt crystallisation is one of the most recurrent damage processes affecting porous building materials worldwide. The durability of building materials with respect to salt crystallisation is often assessed by performing accelerated weathering tests. According to Alves et al. [1], salt weathering tests are the most frequent ageing tests performed in the laboratory, reflecting their worldwide importance for conservation and new construction. A recent literature review on this subject [2] reports a significant variation in the weathering procedures used by researchers. Despite the availability of a European standard [3], three RILEM recommendations [4–6], and a guideline [7], a widely accepted and reliable salt weathering test is still lacking. The use of different test procedures hinders the comparison between the results of different studies.

To tackle this problem, in 2016, the RILEM Technical Committee ASC-271 "Accelerated laboratory test for the assessment of the durability of materials with respect to salt crystallisation" (henceforth referred to as TC ASC-271) was launched to develop an effective laboratory weathering test. The test should reliably assess the durability of porous building materials against salt crystallisation

* Corresponding author.
*E-mail address:* nunes@itam.cas.cz (C. Nunes).

https://doi.org/10.1016/j.conbuildmat.2021.123862
0950-0618/

within a reasonable period, accelerating the deterioration process without significantly altering its mechanism. Since reliable accelerated test procedures for simulating sea-salt spray are already available, e.g., [8,9], the work of TC ASC-271 focuses on developing a procedure that simulates salt damage triggered by capillary transport of salt solution towards the evaporative surface of a material.

TC ASC-271 proposes a new approach to salt crystallisation tests, which differs from existing weathering procedures in this field. In this approach, which is derived from the field of concrete durability [10], as described in Flatt et al. [11], the salt crystallisation damage process consists of two phases: (i) the induction phase, in which salts accumulate in the pores of the material (but the degree of pore filling is not high enough to initiate damage); and (ii) the propagation phase, during which dissolution/crystallisation cycles lead to (increasing) damage (Fig. 1).

Starting from this approach, the new salt crystallisation test, under development by the TC ASC-271, consists of two phases: (1) salt accumulation phase and (2) damage propagation phase. By this approach, not adopted in existing salt crystallization procedures, it is possible to define the risk of decay due to dissolution/crystallization cycles, depending on the salt content (and thus the degree of pore filling) accumulated in the first stage. By separating the two phases, a better understating and forecast of the decay can be achieved.

This paper aims to design the procedure to be followed in the accumulation phase of the salt crystallisation test under development by the TC-ASC-271. The second phase of the test, i.e., the damage propagation phase, is not addressed in this paper. The accumulation phase can be considered successful if it enables the accumulation of salts at the material's evaporative surface (because this is the most common situation observed on site) without the occurrence of damage (damage should only start in the propagation phase).

For the assessment of the capability of the accumulation procedure to fulfil the requirement mentioned above, it is crucial to measure the salt distribution in the specimen at the end of the accumulation phase. This has been done with several methods (destructive and non-destructive), and their advantages and disadvantages are critically discussed.

An extensive literature review of different salt crystallization procedures done by the TC ASC-271 is given in [2]. Standardized tests and procedures proposed by researchers can be classified into two main groups [2]:

- Contamination by capillary absorption or full immersion in a salt solution, followed by drying through one or more evaporative surfaces, e.g., [3–6,13–17], and
- Contamination by continuous capillary absorption of a salt solution and simultaneous drying, the so-called wick action, e.g., [18–21].

In the present work, total immersion of the specimen in salt solution was not tested because it was considered not representative of the salt weathering mechanism occurring in natural exposure conditions [20]. Moreover, full immersion would not be suitable for assessing materials treated with surface treatments or for a combination of materials, such as brick/stone/plaster combinations [2]. Regarding the partial immersion procedure, the contamination can be done repeatedly with salt solution [e.g., 3] or by introducing salts only in the first cycle, followed by rewetting with pure water, e.g., [22]. In the present work, the partial immersion test considered both cases. However, rewetting with pure water was done to mobilize the salts towards the evaporative surface and not to propagate damage.

Existing standards and recommendations prescribe the use of single salt solutions [3–6], usually sodium sulphate or sodium chloride, though, in natural exposure conditions, mixtures of salts prevail. Some researchers choose the composition of the salt mixture based on the analysis of salts present in the building materials on site to reproduce better a specific field condition [23,24]. However, a standard test can hardly consider the use of salt mixtures because this would require different thermohygrometric conditions to make it effective in other materials, which would make impossible any direct comparisons. Moreover, the action of single salts can prove more aggressive than salt mixtures [25,26]. Hence, the present work considers the use of single salt solutions, following existing standards and recommendations.

The salt solution concentration plays a crucial role in the type and severity of damage [27]. The use of solutions with a very high salt content is common in salt crystallisation tests but can lead to unrealistic damage types and severity, e.g., [28]. The KIK-IRPA database encompassing more than six thousand samples collected from buildings in Belgium records salt contents of ca. 1 to 2 wt% with respect to the dry weight of the sample collected onsite [29]. Therefore, in the present study, a realistic amount of salt was introduced in both materials tested (1 wt% of the dry weight of the stones).

The most common methods for the assessment of salt damage in laboratory tests consist of visual and photographic examination and mass loss determination [3–6]. Mass loss is a standard method for assessing damage in durability experiments and has also been used as a parameter for evaluating salt crystallisation durability estimators by several authors, e.g., [15,30,31]. However, this method does not allow obtaining information on damage and salt

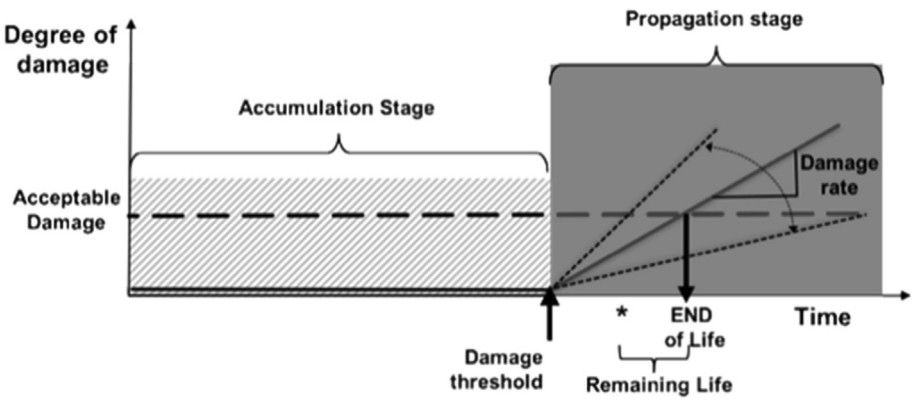


**Fig. 1.** Schematic representation of durability of a stone, subject to salt damage, adapted from the concept proposed by Tuutti [10] to describe the durability of reinforced concrete (image from [11] provided by Robert J. Flatt (ETH Zurich).

distribution inside the specimens. To this scope, other methods and techniques can be used.

Ultrasonic pulse velocity (UPV) measurement is a simple non-destructive technique used to evaluate the physicomechanical properties and the extent of weathering of building materials. UPV can provide information about dynamic mechanical properties, porosity, and the presence of discontinuities in the material [32]. As a result of the salts filling the pores, an increase of the UPV is recorded [33], so this technique can be used to assess salt distribution non-destructively. The drilling resistance measurement system (DRMS) and the scratch tool (ST) are micro-destructive techniques that have been used successfully to monitor the salt crystallisation front in salt weathered limestone, both in the laboratory and in situ, by recording increased cutting resistances in areas where pore clogging due to salt crystallisation occurred [21,34]. The ST uses a diamond cutter to make a scratch (groove) on the surface of the specimen while the cutting force is recorded. The resistance of the material to cutting is related to its physicomechanical properties; in fact, the intrinsic specific energy, which is the energy required for scratching a unit volume of material, is directly proportional to the uniaxial compressive strength of the material [35]. The DRMS operation is similar to the ST, but instead of linear cutting, the DRMS employs rotational cutting (drilling).

Soluble salts are generally hygroscopic, i.e., they can adsorb moisture from the air when the relative humidity (RH) is higher than the RH of equilibrium of the salt. In contrast, most building materials are only weakly hygroscopic. Therefore, by measuring the hygroscopic moisture content (HMC) of a material at high humidity, an indication of the presence of soluble salts can be attained. In the case of single salts, the water activity is known; thus, a fixed relation between the salt content and the HMC at equilibrium can be readily determined at a specific temperature [36,37]. In the case of a salt mixture, several RH equilibrium values are possible, which shift depending on the ionic composition [38]. The HMC method uses powder drilled samples, so it can be combined with the DRMS method, provided that the drilling is performed at different depths within the same drilling hole.

The determination of the salt content within building materials in practice usually consists of extracting the soluble salts with water and analysing the ion content of the leached solution. For a semi-quantitative evaluation of the salts, the HMC method can be used, whereas ion chromatography identifies the ions and provides an accurate quantitative analysis [37].

μ-Xay fluorescence mapping is an elemental technique that allows examining small specimen areas and the production of elemental maps, with a spatial resolution on the micrometre scale. It can provide the excitation of at least one measurable characteristic X-ray peak for all periodic table elements with an atomic number higher than 11. Hence, the method can be applied to detect common ions present in soluble salts affecting building materials, e.g., chloride (atomic number: 17) and sulphur (atomic number: 16). The direct observation of specimens with SEM enables examining the spatial distribution, the morphological character of the salt crystals, and the size of pores in which the salt preferentially crystallizes.

The techniques mentioned above have been used in the present study to evaluate the effectiveness of the designed contamination procedures in accumulating salts close to the evaporative surface. The effectiveness of the methods used is hereby critically discussed.

## 2. Experimental

### 2.1. Contamination procedures

Two types of salt contamination procedures have been selected for this study and are described in detail below. A scheme depicting the two procedures is shown in Fig. 2. After the accumulation phase tests, the specimens were split into two halves for the analysis described in section 2.2., except for the specimens subjected to UPV measurements.

#### 2.1.1. Capillary absorption followed by drying

In this procedure, the specimens were first contaminated from the bottom by capillary absorption with a salt solution, followed by drying only through the top surface at 20 °C and 10% RH, until 80 wt% of the solution evaporated (Fig. 2.a). Two additional wetting/drying cycles with pure water (with the same amount of water used in the salt contamination step) were carried out to move the salts even closer to the evaporative surface.

For both the salt contamination and rewetting steps, the salt solution (or water) was poured into a contamination dish with glass rods. The bottom surface of the specimen was placed in contact with the solution until the top surface was completely wet. After contamination or rewetting, the bottom of the specimen was sealed with parafilm, and the specimen was left to dry only through the top surface.

The quantity of solution (or water) used was similar to the capillary moisture content, i.e., the amount of water absorbed by the specimen at satiation (i.e., to wet the top surface), following capillary rise from its bottom. As mentioned, the concentration of the solution was calculated so that, for both stones, a content of 1 wt % of salt with respect to the dry weight of the specimens was

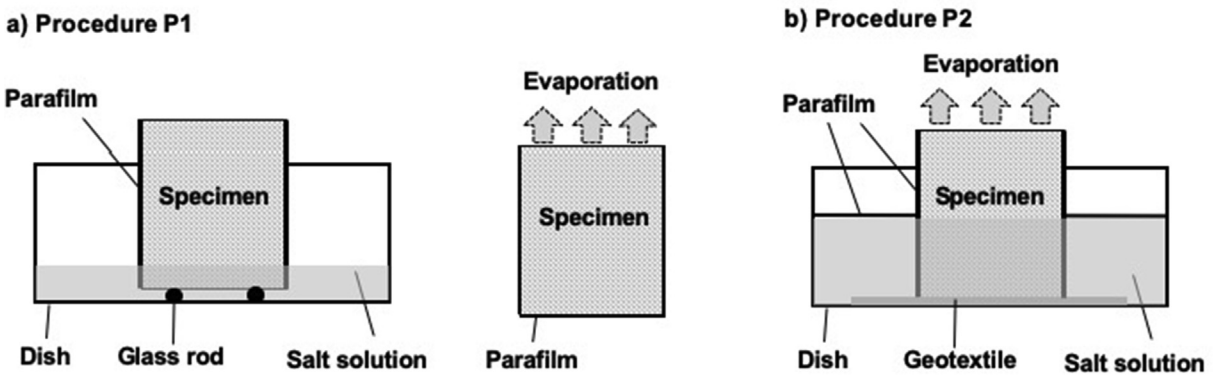


**Fig. 2.** Experimental setup used in the contamination experiments: (a) capillary absorption followed by drying (P1), (b) continuous capillary absorption (P2).

reached. Hence, a salt solution concentration of 6.7 wt% was used for Migné stone, and 3.8 wt% was used for Maastricht stone.

This procedure was performed with three groups of three specimens of each stone to assess the effect of subsequent wetting/drying cycles on salt accumulation:

1) a group of three specimens was subjected only to one drying cycle, following salt contamination; specimens contaminated according to this test are henceforth referred to as **P1-1S**;
2) a group of three specimens was subjected to salt contamination, followed by one rewetting step with water and subsequent drying; specimens contaminated according to this test are henceforth referred to as **P1-1 W;** and
3) a group of three specimens was subjected to salt contamination, followed by two rewetting steps with water and subsequent drying; specimens contaminated according to this test are henceforth referred to as **P1-2 W**.

At the end of the tests, the specimens were further dried at 60 °C in a ventilated oven to constant mass before assessing the salt distribution.

*2.1.2. Continuous capillary absorption*

In this procedure, the salt solution was poured into a contamination dish with a geotextile layer on the bottom (ca. 1 mm thick), and the bottom of the specimen was placed in contact with the solution (Fig. 2b). The amount of water used in the preparation of the solution was the same as the total amount of water used in procedure P1-2 W, i.e., the sum of water used during the initial salt contamination (P1-1S) plus the water used in the two following rewetting cycles to achieve the same amount of salt (1 wt%) with respect to the dry weight of the specimens.

Drying occurred only through the top surface of the specimen at 20 °C and 10% RH. Evaporation of the solution from the dish during the test was prevented by covering it with a parafilm sheet. After complete absorption of the salt solution, the bottom of the specimens was sealed, and the specimens were left to dry (20 °C and 10% RH) until 80 wt% of the water absorbed evaporated. Afterwards, the specimens were dried at 60 °C to constant mass before assessing the salt distribution.

## 2.2. Materials

*2.2.1. Salt types*

Two salt types, sodium chloride (NaCl) and sodium sulphate ($Na_2SO_4$), have been used. This selection was based on the following criteria:

- Both salts are commonly found in buildings worldwide and are known to cause severe damage.
- These salts have different crystallisation behaviour. $Na_2SO_4$ has temperature-dependent solubility and multiple polymorphs (hydrate and anhydrous forms) at ambient temperature. In contrast, NaCl solubility is almost independent of temperature, and NaCl has no hydrate forms at temperatures higher than 0 °C.

$Na_2SO_4$ is generally more damaging than NaCl in laboratory weathering tests. Moreover, these salts are the most commonly used in crystallisation tests [2].

*2.2.2. Stone types*

Migné stone (quarried in France) and Maastricht stone (quarried in The Netherlands) were used in the tests. These limestones have been chosen because of their similar chemical composition (both stones are composed of ca. 95–99% of calcite), their homogeneous structure without macroscopically evident bedding planes, their unimodal pore size distribution, and their significantly different porosity and pore size. Table 1 presents the main physical properties of the stones. The open porosity of Migné is ca. 30% and that of Maastricht is ca. 50%. The grain size is homogeneous: ca. 100–150 μm for Maastricht and 1–5 μm for Migné. Maastricht has a main pore size of ca. 30 μm, whereas Migné has a main pore size of ca. 1 μm. The difference in pore size is reflected in the rate of water absorption by capillarity: Maastricht's water absorption coefficient is an order of magnitude higher than that of Migné [12].

*2.2.3. Specimen preparation and testing conditions for both procedures*

Cylindrical specimens (Ø 50 mm, height 50 mm) were cut from a large stone block in such a way that the bedding planes of the stone laid parallel to the top and bottom surfaces of the specimen. The specimens were sealed along their side surface with parafilm after pre-heating them in an oven at 50 °C for 10 min to achieve better adherence. A textile tape was used to glue the end of the parafilm foil and ensure sealing tightness during the entire test. Before contamination, the specimen mass was stabilized at 20 °C and 10% RH, which were the conditions used during the contamination and drying phases. Low temperature, RH, and negligible air flow conditions were set to promote the accumulation of salt close to the evaporative surface.

For each procedure, a group of three specimens of each stone was contaminated with a salt solution of NaCl and another group with $Na_2SO_4$; both salts were ACS reagents $\geq$ 99.0%. The concentration of the salt solution used for the contamination was defined according to the desired salt content in the specimen, which was 1 wt% of its dry weight. The same salt content was used in both procedures to enable direct comparison of the results.

A ventilated climatic chamber (Vötsch VC 4018) was used to provide constant thermo-hygrometric conditions. Throughout the tests, the specimens were placed in the climatic chamber inside plastic boxes (40 × 34 × 17 cm, three specimens per box), with the opening covered with Japanese silk paper (ca. 15 g/m$^2$) to prevent air flow. Digital thermo-hygrometers (Comet S3621) were placed inside the boxes to monitor the RH, which resulted in being 13 ± 3%.

## 2.3. Assessment of damage and salt distribution

At the end of the accumulation phase, the occurrence of damage and salt efflorescence was visually and photographically recorded. During the accumulation phase, the salt introduced should remain in the specimens, i.e., not crystallise as salt efflorescence, and damage should ideally be absent or of low intensity. Hence, both the amount of salt efflorescence and mass loss were used to assess the suitability of the procedures to be used in the accumulation phase.

Several analytical methods (destructive and non-destructive) were used to assess the salt distribution: ion chromatography (IC), hygroscopic moisture content (HMC), micro X-ray fluorescence (μ-XRF), scanning electron microscopy (SEM), drilling resistance measurement system (DRMS), scratch tool (ST), and ultrasonic pulse velocity (UPV).

**Table 1**
Properties of Migné and Maastricht limestones [12].

| Properties | Maastricht | Migné |
|---|---|---|
| Open porosity (%) | 53.1 ± 0.4 | 32.4 ± 0.5 |
| Main pore size - Hg volume (μm) | 30.4 ± 0.2 | 0.95 ± 0.05 |
| Water absorption capillary coefficient (g/cm$^2$/min$^{0.5}$) | 2.19 ± 0.16 | 0.23 ± 0.01 |

After the accumulation phase tests, the specimens were split into two halves, using a hammer and chisel, for analysis with the mentioned methods, except for the specimens subjected to UPV measurements. Fig. 3 shows a scheme summarizing the number and type of specimens and respective analyses performed with each method of assessment of salt distribution.

*2.3.1. Visual observations and mass variation*

The development of salt efflorescence and damage was monitored photographically. Since salt efflorescence can hide the underlying damage, photographs were taken before and after removing the efflorescence. The type and severity of damage types, when present, were described according to the ICOMOS glossary [39] and MDCS atlas [40].

The weight of the specimens was recorded before and after salt contamination; based on this, the exact amount of salt introduced in each specimen was calculated. During the drying phase of both procedures, the weight of the specimens was recorded at regular intervals until 80 wt% of the water had evaporated. The damage was assessed by recording the mass loss.

At the end of the test, the salt efflorescence and stone debris, when present, were collected using a soft brush and weighed using a balance (resolution of $10^{-4}$ and accurate to $10^{-3}$g). The salt efflorescence was separated from the stone debris by dilution in pure water, followed by filtration with filter paper. The weight of the debris was measured, and that of the salt was calculated. Salt that might have accumulated in the pores of the stone debris collected was hence registered as salt efflorescence.

*2.3.2. Ion chromatography (IC)*

For the analysis of the salt content (NaCl or $Na_2SO_4$), measurements were carried out on drilled powder samples. For each half-core specimen, starting from the evaporative surface, samples were collected up to the following depths (same hole): 0–5, 5–10, 10–15, 15–20, 20–30, 30–40, and 40–50 mm. Additionally, to get more precise information on the salt distribution in the salt-rich outer layer, samples were collected by sanding down a half-cylinder at 1 mm intervals up to 5 mm depth per specimen.

The quantity of anions ($Cl^-$ and $SO_4^{2-}$) and cations ($Na^+$) of the vacuum filtered extract was analysed by IC (Metrohm). The results in parts per million (ppm – mg/L) were converted to wt.% (relative to the dry sample weight), and the sum of the equimolar contents of $Na^+$ and $Cl^-$ or $SO_4^{2-}$ was estimated. The salt amount present in each layer was calculated as the percentage of the total salt content present in the sample. The average amount of each ion (in wt.%) in each group of three specimens contaminated with each procedure was calculated in relation to the respective total weight of each group of samples.

*2.3.3. Hygroscopic moisture content (HMC)*

For the determination of the HMC, the same samples used in the IC analysis were placed in a climate chamber at 20 (±1) °C and 95% (±3) RH until constant weight (41 days). The HMC was calculated according to the equation:

$$HMC = 100 \cdot \frac{\Delta m}{m_d} \quad (1)$$

in which $\Delta m$ represents the mass gain of the sample (g), and $m_d$ represents the dry weight of the sample (g).

The correlation between the HMC values (wt.%) and the salt content (wt.%) was determined considering a dataset of 292 drilled samples. The salt content considered was limited to equimolar contents derived from the IC analysis of samples containing $Na^+$ and $Cl^-$ or $Na^+$ and $SO_4^{2-}$. The correlation coefficient indicates how well the data fits the model of regression and is presented as $R^2$, calculated according to the following equation:

$$R^2 = \left( \frac{n(\sum xy) - (\sum x)(\sum y)}{\sqrt{\left[n\sum x^2 - (\sum x)\right]^2 \left[n\sum y^2 - (\Sigma y)^2\right]}} \right)^2 \quad (2)$$

in which $\times$ corresponds to the value of HMC (wt.%), and $y$ corresponds to the salt content (wt.%).

*2.3.4. Micro X-ray fluorescence mapping (μ-XRF)*

Chloride and sulphur μ-XRF maps were produced to check the NaCl and $Na_2SO_4$ distribution, respectively. The instrument used for the μ-XRF analysis was an EDAX (Mahwah, NJ, USA) ORBIS μ-XRF spectrometer. The system uses a Silicon Drift Detector (SDD). It focuses the X-rays from a rhodium target anode with a

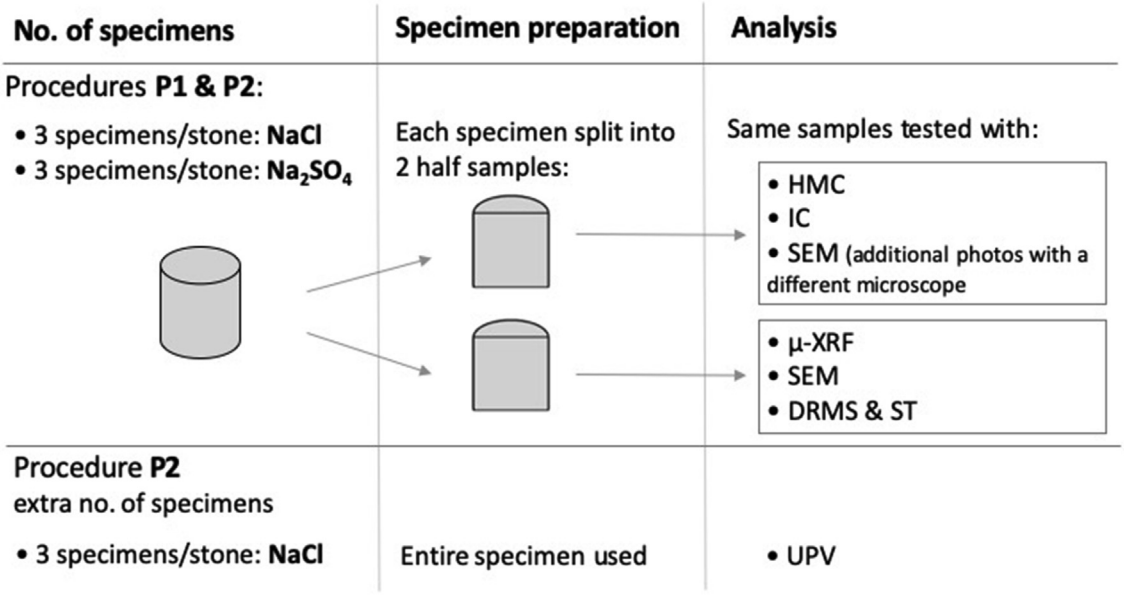


**Fig. 3.** Summary of the number and type of specimens tested with each procedure and analysis performed.

poly-capillary focusing optic, which allows for a beam diameter of ca. 30 μm. The acquisition system is the ORBIS Vision Software supplied by EDAX. The applied acceleration potential and current were 35 kV and 500 μA, respectively. At each point, every 100 μm (spacing), a spectrum was acquired for 100 ms (30%-40% dead time). The measurements were carried out at atmospheric conditions with a built-in 25-μm thick aluminum filter to eliminate the rhodium Lα radiation, which overlaps with the chlorine Kα X-ray line and increases its limit of detection.

A smooth surface is required for this analysis, so prismatic specimens were dry-cut from the half cores along their longitudinal axis. The selected surface of 5x5 cm to be mapped was ground with SiC paper (STRUERS 500) for 15 s, at 300 rpm, in a single direction to avoid spreading the salt.

*2.3.5. Scanning electron microscopy (SEM)*

SEM observations were carried out on the same samples analysed with μ-XRF. Polished sections were produced from 2 × 2 cm pieces of stone. The samples were prepared in the same way as those prepared for the μ-XRF analysis but were further embedded under vacuum in low viscosity epoxy resin (EPO-TEK). After 24 h of polymerization, the specimens were grinded with SiC paper (STRUERS) at 500, 1000, 2400, and 300 rpm for 5 min (each step), using isopropanol as coolant. The final polishing was carried out with water-free diamond polishing suspensions (9, 3, and 1 μm). Polished surfaces were coated with a 15 nm carbon layer, then observed with an SEM FEI QUANTA 200 3D, at high vacuum, and 20 kV voltage.

Additional samples from Maastricht limestone contaminated with $Na_2SO_4$ according to procedure P1-1S (belonging to the same set analysed with IC and HMC) were studied with a Zeiss Gemini 300 SEM FE equipped with an Oxford X-Max detector at high vacuum and 15 kV voltage. Polished cross-sections were prepared by embedding the stone fragments in bi-component epoxy resin (Epo-Fix, Struer), grinding them with SiC paper (Struers), and polished with polishing cloth up to 8000 grit. Isopropanol was used during grinding and polishing to avoid salt dissolution. The salt distribution within the stone matrix was mapped up to a 2.5 mm depth from the evaporative surface by combining multiple images acquired in constant conditions (back-scattered mode) at 150x magnification.

*2.3.6. Drilling resistance measurement system (DRMS) and scratch tool (ST)*

Samples contaminated according to procedure P1, and previously mapped with μ-XRF, were scratched and drilled to assess the position of the salt crystallisation front. Non-contaminated Migné and Maastricht samples were also used as a reference.

Scratching was performed using a WOMBAT Scratch Tool supplied by Epslog Engineering. The samples were scratched along the centre of their curved side, moving from the evaporative surface towards the base. A sharp rectangular 10 mm wide diamond cutter with a negative back rake angle of 15°, moving at constant velocity (10 mm/s), was used in all the scratch tests. During scratching, the normal ($F_n$) and tangential ($F_t$) components of the total force required to form a groove on the sample were recorded automatically. From these, the total cutting force ($F$) was estimated as [29]:

$$F = \sqrt{(F_n^2 + F_t^2)} \quad (3)$$

For the DRMS test, the samples were drilled starting at the evaporative surface of the samples using a device supplied by SINT Technology. The operating conditions during drilling were 600 rpm for the rotational speed and 10 mm/min for the penetration rate. A twist diamond drill bit with a flat point and Ø 5 mm was used; the total penetration depth was 10 mm. During the drilling tests, the DRMS provided a continuous reading of the force required to perforate the test specimen.

*2.3.7. Ultrasonic pulse velocity (UPV)*

UPV measurements were performed to assess the salt distribution non-destructively, using a portable instrument (USG 20 Krompholz Geotron Elektronik (DE)) with pointy-ended transducers with a contact section of Ø 3 mm. Only specimens contaminated according to procedure P2 were measured; for this test, three extra cylindrical specimens of each stone were used. Nine measurements were performed in each specimen in planes parallel to the evaporative surface at 5 mm intervals. The measurements were performed before and after salt contamination.

## 3. Results

### 3.1. Damage and salt efflorescence

A summary of the visual observations, focusing on the qualification of salt efflorescence and damage on the specimens contaminated with both procedures, is shown in Figs. 4 and 5. The amount of salt efflorescence and mass loss are given in Figs. 6 and 7, respectively. In the case of procedure P1, the debris of the specimens subjected to further rewetting steps was only collected at the end-step, so the results shown are cumulative.

Samples contaminated with NaCl with both procedures developed only salt efflorescence, and no visible damage was detected (Fig. 4). The type and amount of salt efflorescence (Fig. 6a) varied according to the procedure followed and type of stone used: a lower amount of NaCl efflorescence developed in the less porous stone (Migne) with procedures P1-1S and P2, but the amount was still slightly higher than for the more porous stone (Maastricht) with procedures P1-1 W and P1-2 W. The results of mass loss (Fig. 7a) can be considered negligible (lower than 0.05 wt%) and confirm the visual observations.

Both types of stones contaminated with $Na_2SO_4$ showed damage with all procedures (Fig. 5). Minor damage was observed in Migné after $Na_2SO_4$ contamination with procedure P1-1S, leading to ca. 1 wt% of mass loss (Fig. 7b); the amount of salt efflorescence observed was very low and concentrated close to the evaporative surface. After one rewetting, $Na_2SO_4$ contaminated Migné specimens (P1-1 W) suffered rapid and severe damage (within 24 h of drying). For this reason, the planned second rewetting was not performed, and these specimens were not subjected to the analysis of salt distribution.

In the case of the more porous stone (Maastricht), samples contaminated with $Na_2SO_4$ with procedure **P1-1S** developed slight granular disintegration and scaling, leading to 0.7 ± 0.4 wt% mass loss (Fig. 7b). After one rewetting (**P1-1 W**), the amount of salt efflorescence increased significantly; the amount of efflorescence reached almost 90 wt% of the salt introduced, whereas mass loss was ca. 1.1 wt%. The 2nd rewetting step (**P1-2 W**) induced more damage (ca. 2 wt% of mass loss) and slightly more salt efflorescence. In contrast with Migne, damage occurred in Maastricht samples contaminated with $Na_2SO_4$ with procedure **P2.**

The period for the evaporation of 80% of the water introduced during the contamination varied according to the stone type, salt type, and procedure (Table 2). As expected, samples with higher porosity and pore size dried faster. The drying period with procedure P2 was more prolonged than with procedure P1-1S for both stones contaminated with either salt. This aspect can be attributed to the higher degree of saturation of the porous system of the stones with procedure P2, resulting from the continuous capillary

| Procedure | | Migné - NaCl | Maastricht - NaCl |
|---|---|---|---|
| **P1-1S** | Photo | 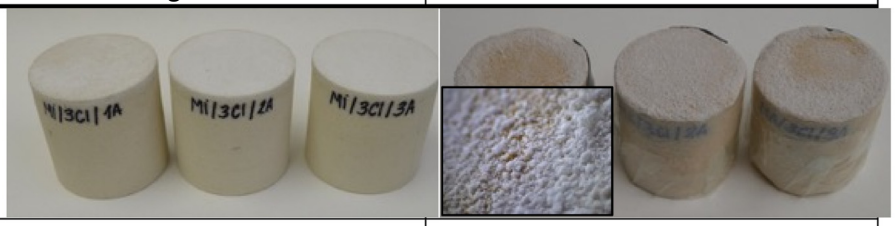 | |
| | Damage/alteration | Efflorescence | Efflorescence |
| | Salt efflorescence | Powdery | (micro) cauliflower |
| | Damage severity | No damage | No damage |
| | Damage extension | - | - |
| **P1-1W** | Photo |  | |
| | Damage/alteration | Efflorescence | Efflorescence |
| | Salt efflorescence | Powdery (surface) and hollow crust | Powdery |
| | Damage severity | No damage | No damage |
| | Damage extension | - | - |
| **P2-2W** | Photo | 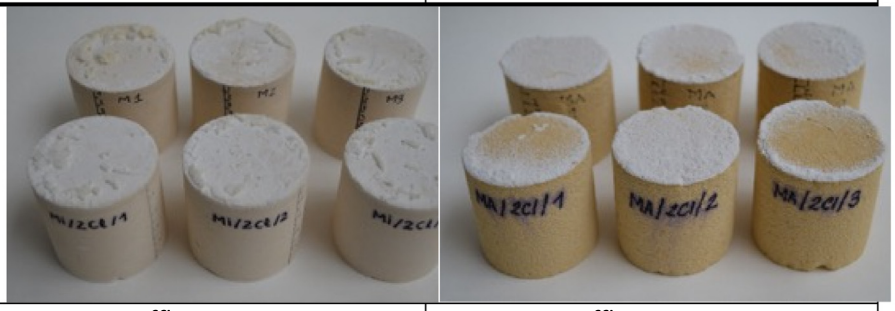 | |
| | Damage/alteration | Efflorescence | Efflorescence |
| | Salt efflorescence | Powdery | Powdery |
| | Damage severity | No damage | No damage |
| | Damage extension | - | - |

**Fig. 4.** Summary of the macroscopic visual observations on the specimens contaminated with NaCl. Scores of severity of damage: low (+) to high (++++). Scores of extension of damage: small (+) to large (++++) surface area.

absorption of a solution with two times higher amount of water than procedure P1-1S.

### 3.2. Assessment of the salt distribution

#### 3.2.1. Ion chromatography (IC) and hygroscopic moisture content (HMC)

The salt distribution assessed with IC is presented in Figs. 8 and 9. Generally, salt accumulated close to the evaporative surface and the salt content decreased with depth. The salt content in the outer 5 mm layer was always above 50 wt% of the total content, except in the case of **Maastricht** contaminated with **$Na_2SO_4$** with procedure **P1-1S** (Fig. 9b). In this case, the amount of salt present in the outer 5 mm layer was lower than ca. 30 wt%, but the standard deviation was large.

Different results were obtained when the samples were rewetted; the salt content up to 5 mm depth slightly increased or decreased after one rewetting (**P1-1 W**) for Migné and Maastricht contaminated with **NaCl**, respectively. Subsequent rewetting of Migné stone contaminated with NaCl (**P1-2 W**) led to an increment of efflorescence and salt in the 0–5 mm layer. In Maastricht, the amount of salt efflorescence decreased with subsequent rewetting (ca. 30 wt%), while the salt content in the 0–5 mm layer increased. **Maastricht** contaminated with **$Na_2SO_4$** with **P1-1 W** showed an increment of the salt content in the outer layer (0–5 mm); rewetting twice (**P1-2 W**) led to an increment of efflorescence and a decrease of the salt content in the outer layer. These results are possibly related to the removal of the damaged salt-rich layer after brushing the specimens contaminated with **P1-2 W**. Upon rewetting (P1-1 W and P1-2 W), salts were transported towards the evaporative surface; consequently, the salt content in the outer 5 mm layer and/or the amount of efflorescence increased.

A more detailed analysis was carried out on the first 5 mm of a sample of **Maastricht** contaminated with **$Na_2SO_4$** according to procedure **P1-1S** (Fig. 10). The results indicate that 73.5 wt% of the total salt content was located within the first millimetre of the

| Procedure | | Migné – Na2SO4 | Maastricht – Na2SO4 |
|---|---|---|---|
| P1-1S | Photo | 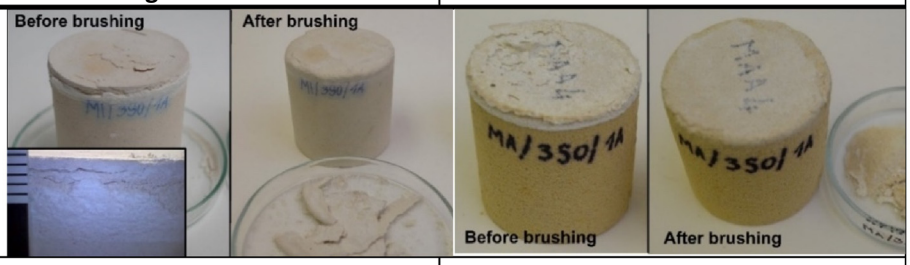  | |
| | Damage/alteration | Scaling with subflorescence | Efflorescence, granular disintegration, and scaling with subflorescence |
| | Salt efflorescence | Powdery | Powdery |
| | Damage severity | ++ | ++ |
| | Damage extension | ++ | ++ |
| P1-1W | Photo | 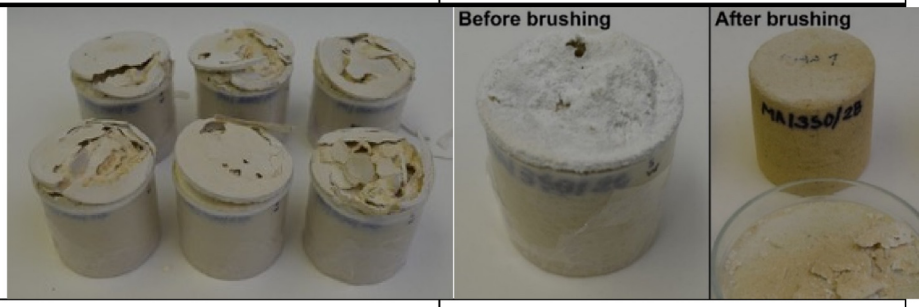  | |
| | Damage/alteration | Bursting with subflorescence | Granular disintegration with subflorescence |
| | Salt efflorescence | Crust | Crust |
| | Damage severity | ++++ | ++ |
| | Damage extension | ++++ | ++++ |
| P2 | Photo | 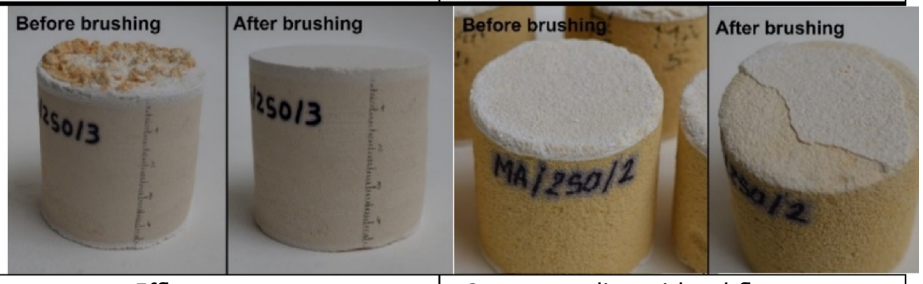  | |
| | Damage/alteration | Efflorescence | Contour scaling with subflorescence |
| | Salt efflorescence | Cauliflower | Powdery |
| | Damage severity | + | ++ |
| | Damage extension | + | ++ |

**Fig. 5.** Summary of the macroscopic visual observations on the specimens contaminated with $Na_2SO_4$. Scores of severity of damage: low (+) to high (++++). Scores of extension of damage: small (+) to large (++++) surface area.

specimen. Deeper in the stone, the concentration dropped significantly, with 16.8 wt% between 1 and 2 mm, and 2.6 wt% between 4 and 5 mm. Considering the open porosity, bulk/skeletal density of the stone, mass of salt in the stone, molar mass/volume of thenardite or phase III, it is possible to estimate that 10% of the volume of the pores in the outer 1 mm were filled with salt (assuming a homogeneous distribution of salt, including a thin salt crust on the surface of the sample).

The salt distribution results obtained with HMC are in line with those measured by IC. The correlation of determination between HMC and IC salt content was used in this study to check whether HMC could give reliable semi-quantitative results. Considering 168 samples with a wide range of salt contents (Fig. 11a), a good correlation was derived ($R^2$ = 0.9305). However, when considering a salt content below 1 wt% (144 samples), the correlation dropped significantly ($R^2$ = 0.6175) (Fig. 11c). In samples with such a low salt content and weight (ca. 0.928 g), the experimental error increases. Next to the experimental error, minimal changes in RH in the climatic chamber can have a significant impact on the HMC values, especially in the case of high RH and hygroscopic salts, such as NaCl.

### *3.2.2. Micro X-ray fluorescence mapping (μ-XRF) and scanning electron microscopy (SEM)*

A summary of the observations from μ-XRF maps and SEM images is presented in Table 3. Fig. 12 gives an example of the

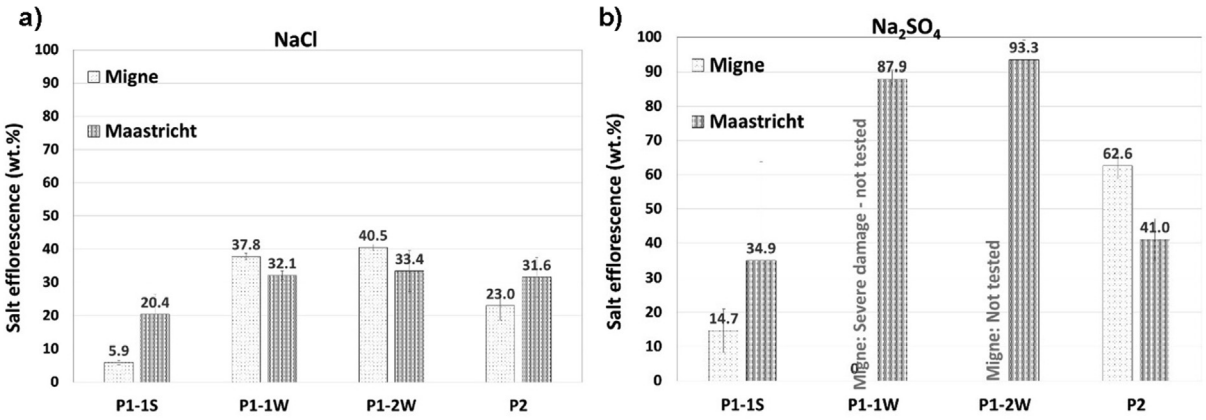


**Fig. 6.** Mass of salt efflorescence registered after the salt accumulation test with procedures P1 and P2 expressed as the percentage relative to the total salt amount introduced in the specimens: (a) stones contaminated with NaCl, (b) stones contaminated with $Na_2SO_4$.

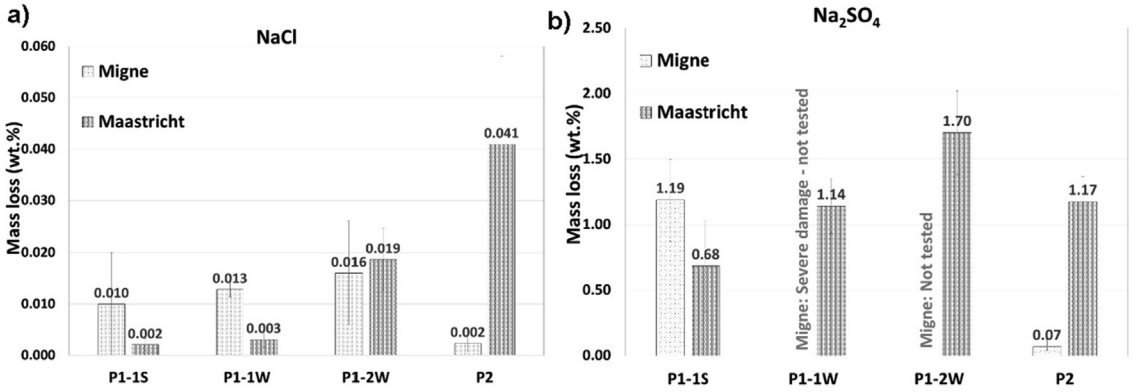


**Fig. 7.** Mass loss of stone material registered after the salt accumulation test with procedures P1 and P2, expressed as the percentage relative to the dry weight of the specimens: (a) stones contaminated with NaCl, (b) stones contaminated with $Na_2SO_4$.

**Table 2**
Period (in days ± 3) for evaporation of 80% of the water introduced during the contamination.

| Procedure | Migné | | Maastricht | |
|---|---|---|---|---|
| | NaCl | $Na_2SO_4$ | NaCl | $Na_2SO_4$ |
| P1 −1S | 37 | 24 | 10 | 10 |
| P1 −1W & 2 W | 21 | – | 8 | 8 |
| P2 | 40 | 30 | 12 | 12 |

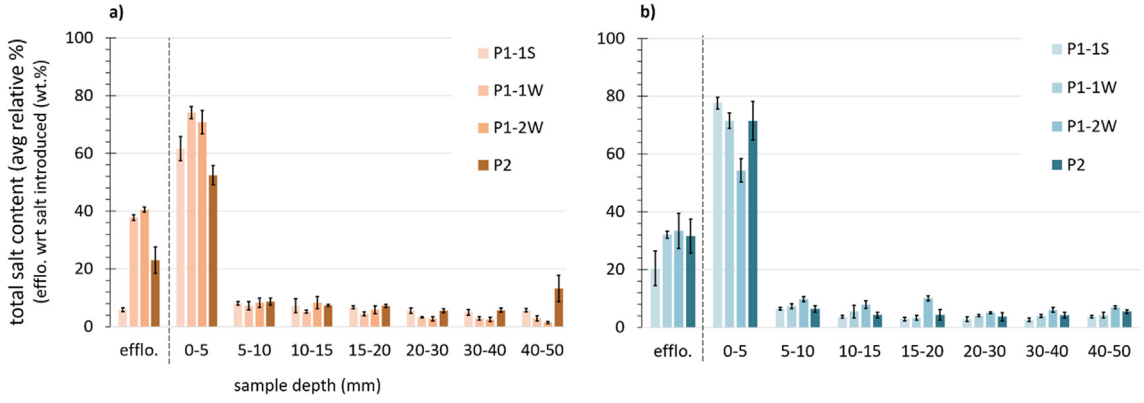


**Fig. 8.** Mean relative percentage of NaCl distribution assessed with IC in Migné (a) and Maastricht (b) after contamination with procedures P1 and P2. The values are the average of 3 specimens; the graphs include the amount of salt efflorescence (efflo). The legend from top to bottom represents the different procedures, which sequentially correspond to the columns from left to right.

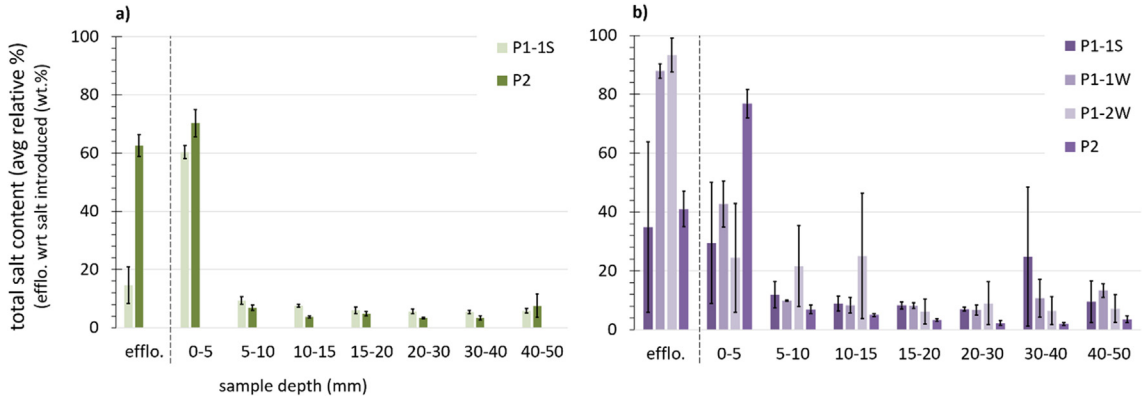


**Fig. 9.** Mean relative percentage of $Na_2SO_4$ distribution assessed with IC in Migné (a) and Maastricht (b) after contamination with procedures P1 and P2. The values are the average of 3 specimens; the graphs include the amount of salt efflorescence (efflo). The legend from top to bottom represents the different procedures, which sequentially correspond to the columns from left to right.

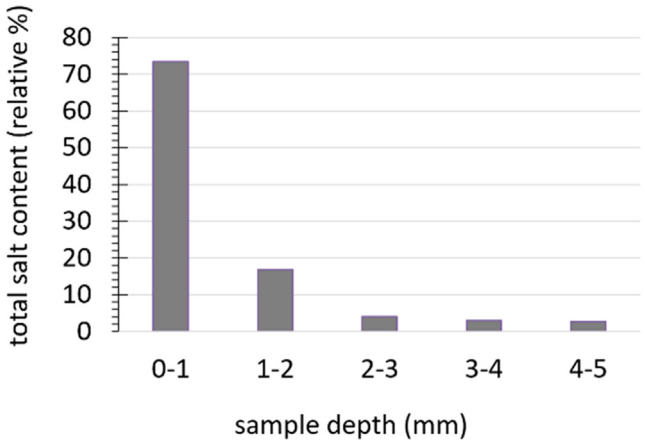


**Fig. 10.** Relative percentage of $Na_2SO_4$ distribution in the first millimetres of Maastricht contaminated with procedure P1-1S.

μ-XRF maps recorded in Migné and Maastricht contaminated according to procedure P1 with NaCl. Figs. 13, 14, 15, and 16 show a few selected SEM microphotographs.

The results indicate that procedure **P1-1S** is the most effective in accumulating salt at the evaporative surface of both stones. In general, rewetting reduces the thickness of the salt layer and promotes the redistribution of salts deeper into the samples. The data also indicated that NaCl is more prone to be redistributed within the sample thickness of both stones upon rewetting. Procedure **P2** also showed a salt layer at the evaporative surface in both stones, with either salt; NaCl further spread within the sample thickness.

SEM gives a more precise assessment of the thickness of the salt layer and salt distribution than the μ-XRF maps, although the salt distribution can be quite non-homogeneous. Therefore, a thickness interval is probably more appropriate rather than a single value. The representativeness of the sample observed with SEM can also be an issue; e.g., no salt layer was observed under SEM with Maastricht contaminated with procedure P1-1S with NaCl, but a salt layer up to 1 mm thickness was observed in the μ-XRF maps.

The additional SEM analysis of Maastricht contaminated with $Na_2SO_4$ with procedure **P1-1S** showed only partial filling of the pore spaces and a higher concentration of the salt close to the evaporative surface. Images of the fresh fracture showed that the salt crystallizes as porous clusters within the inter-particle spaces (Fig. 15). Such a crystallisation pattern was confirmed by the cross-section observation and mapping of the salt distribution (Fig. 16). The salt was mostly concentrated up to 400–500 μm from the evaporative surface, showing a rather irregular distribution. The presence of salt was detected at least up to 2 mm depth, as isolated clusters of salt crystals formed along the grain borders of the stone. These observations are in line with the IC results on the same sample (Fig. 10) in which ca. 70% of the salt was detected up to 1 mm depth and ca. 20% of salt was detected between 1.5 and 2 mm depth.

### *3.2.3. Drilling resistance measurement system (DRMS) and scratch tool (ST)*

The scratching and drilling force (*F*) patterns versus the cutter position (depth of the sample) are provided in Fig. 17. From these, evident changes in the microstructure of the salt contaminated samples (i.e., pore clogging resulting in increased cutting resistance areas) can be observed. In particular, in all the patterns derived after salt contamination and drying, localized peaks in material resistance to cutting were recorded very close to the evaporative surface (ca. 0–2 mm). These peaks, which are not observed in the reference specimens, are prominent both in the ST and the DRMS patterns and suggest pore filling by the salts.

The position of the peaks in cutting resistance is nearly identical for each sample, irrespective of the mapping technique used, indicating that both methods are detecting pore clogging due to salt crystallisation at more or less the same location. This is in line with previous applications of the ST and the DRMS [21,28] and confirms the reliability of both techniques and their potential in detecting the position of the salt crystallisation front in limestone.

The peak cutting resistance recorded in the case of **Migné** contaminated with **$Na_2SO_4$** with procedure **P1-1S** is much higher, compared to the corresponding sample contaminated with **NaCl**. This is in line with the μ-XRF and SEM results (Table 3), which suggest that $Na_2SO_4$ has a tendency to crystallise more locally, closer to the evaporative surface, as opposed to NaCl which shows higher dispersion. The localised crystallisation of $Na_2SO_4$ usually leads to more damage [16], as was indeed the case in the visual observations hereby reported (Figs. 4 and 5). In the case of the much weaker and porous **Maastricht** stone, the peak resistance recorded for the sample contaminated once (**P1-1S**) with **NaCl** was again rather low. Upon rewetting with water (**P1-1 W**), the peak resistance was further reduced. In contrast, the thickness of the salt-rich layer (i.e., increased cutting resistance area) appears broader, albeit not as broad as in the optimised μ-XRF map, suggesting some redistribution of the salt content with water absorption and possibly some salt escaping the sample as efflorescence; this

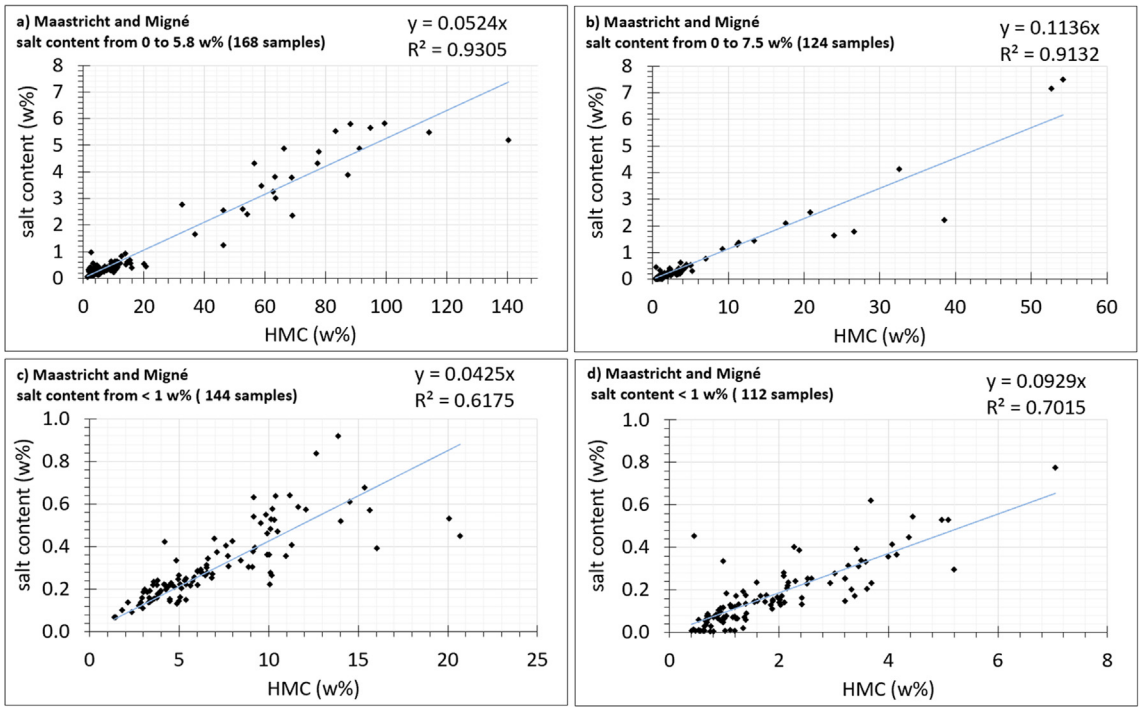


**Fig. 11.** Correlation between HMC values and salt content ($R^2$ = coefficient of determination): Maastricht and Migné with NaCl (a) and $Na_2SO_4$ (b) content (full range detected between 0 and 5.8 or 7.5 wt%) and with NaCl (c) and $Na_2SO_4$ (d) content below 1 wt%.

**Table 3**
Summary of μ-XRF maps and SEM image observations.

| Procedure | Method | Migné - NaCl | Maastricht - NaCl | Migné – $Na_2SO_4$ | Maastricht – $Na_2SO_4$ |
|---|---|---|---|---|---|
| P1-1S | μ-XRF maps | - Cl layer up to 1 mm depth (Fig. 12a)- Cl dispersed throughout the sample (Fig. 12b) | - Cl layer up to 1 mm depth | - S layer up to 1 mm depth | - S layer up to 1 mm depth |
| | BSE images | - Salt layer up to 200–500 μm depth (Fig. 14) | - No salt layer observed- Scattered salt crystals | - Salt layer up to 50 μm depth- Salt crystals up to 2 mm depth | - Salt layer up to 200 μm depth (Fig. 13)- Most of the salt up to 400–500 μm depth.- Scattered salt crystals up to 2 mm depth |
| P1-1 W | μ-XRF maps | - Cl rich layer up to 1 mm depth- Cl dispersed throughout the sample with a slightly higher concentration at the bottom | - Cl rich layer up to 0.5 mm depth- Cl scattered up to 10 mm depth (Fig. 12c, d) | * | - S layer up to 1 mm depth |
| | BSE images | - Salt dense layer up to 200–250 μm depth | - Continuous salt layer up to 400 μm depth | * | - Salt layer up to 150 μm depth |
| P1-2 W | μ-XRF maps | - Cl layer up to 0.5 mm depth | - Cl layer up to 0.5 mm depth | * | - S was not detected |
| | BSE images | - Salt dense layer up to 200–250 μm depth | - Non-continuous salt layer up to 200 μm depth | * | - No salt layer observed |
| P2-2 W | μ-XRF maps | - Cl layer up to 1 mm depth- Cl also dispersed up to 10 mm depth | - Cl layer up to 1 mm depth- Cl also dispersed up to 2.5 mm depth | - S layer up to 1 mm depth | - S layer up to 1 mm depth |

* Not measured (severe damage of the specimen after rewetting).

is in line with the amount of salt efflorescence formed, as well as the IC data (Fig. 8).

### 3.2.4. Ultrasonic pulse velocity (UPV)

The UPV results before and after contamination with **NaCl** with procedure **P2** are shown in Fig. 18; the values given correspond to the percentage change before and after contamination. After salt contamination, a significant UPV increase is observed in Maastricht at 0–10 mm depth from the evaporative surface; UPV values at 5 mm increased by 44%, compared to the same specimen without salt. These results indicate that salt accumulated in the first 5 mm of the specimen. In contrast, a very slight difference in UPV values before and after salt contamination was detected in Migné stone contaminated with NaCl. Fig. 18b) shows only 7% UPV increase after Migné salt contamination; these results suggest that salt has evenly precipitated throughout the depth of the specimen, which is not in line with the IC and HMC results.

## 4. Discussion

### 4.1. Comparison of procedures

A summary of the advantages and disadvantages of the procedures used for salt accumulation (1 wt% with respect to the total

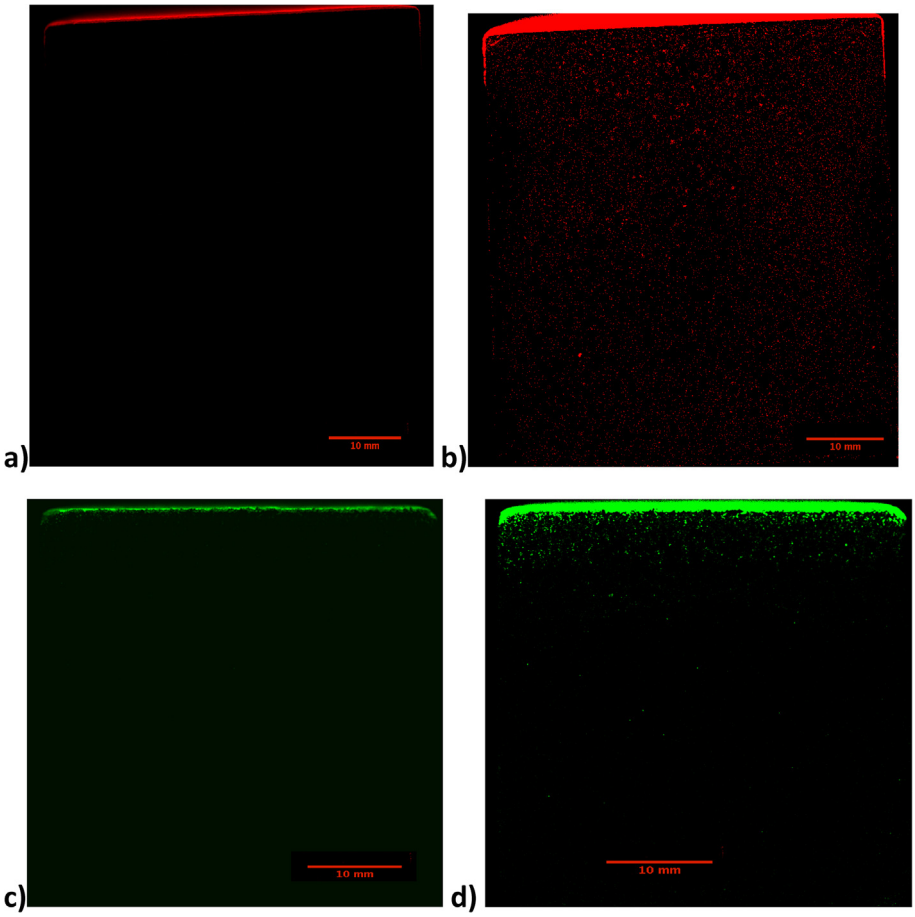


**Fig. 12.** μ-XRF chloride maps of Migné and Maastricht contaminated according to procedure P1. Migné contaminated according to procedure P1-1S: (a) original map, (b) enhanced map by Image J software; the dense red layer on the top of the sample is an image artefact. Maastricht contaminated according to procedure P1-1 W: c) original map, d) enhanced map by image J software; the dense green layer on the top of the sample is an image artefact. (For interpretation of the references to color in this figure legend, the reader is referred to the web version of this article.)

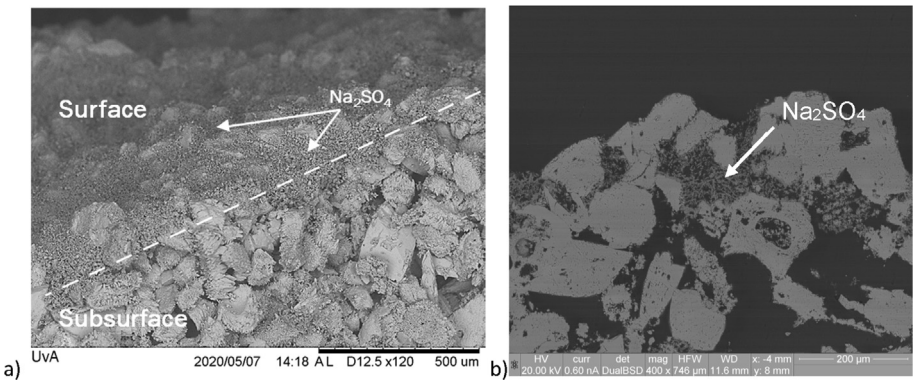


**Fig. 13.** Maastricht contaminated with $Na_2SO_4$ according to procedure P1-1S: (a) SEM image of the ground surface. (b) BSE image on polished section showing a layer of $Na_2SO_4$ crystals filling the interparticle porosity just beneath the evaporative surface (the arrow indicates the location of salt as analysed with EDX). b).

weight of each stone) is presented in Table 4. Procedure **P1-1S** was the most effective in accumulating salts in a thin layer beneath the evaporative surface of the stones without causing too much damage. Rewetting with procedure P1 led to the damage propagation phase in specimens contaminated with $Na_2SO_4$ and redistribution of both salts within the specimens, along with the development of salt efflorescence. Procedure **P1-1S** with **NaCl** promoted less salt efflorescence in both stones than with **$Na_2SO_4$**, whereas procedure **P2** caused a higher amount of salt efflorescence in both stones with each of the salts.

The results of the assessment of the salt distribution showed that in all procedures, most of the salt is concentrated in the first millimetres of the subsurface. Stones contaminated with **NaCl** according to procedure **P1-1S** showed higher salt content in the

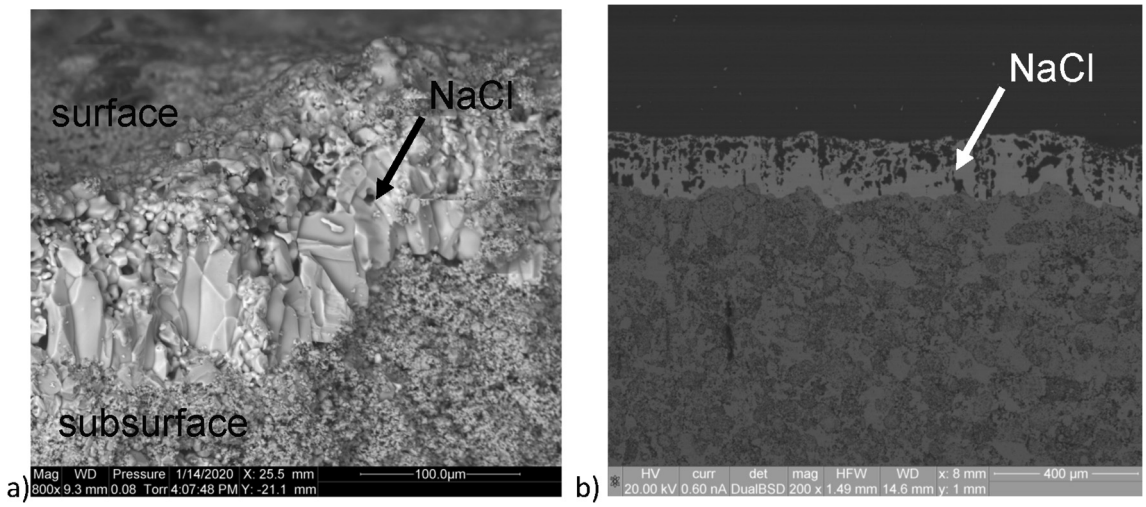


**Fig. 14.** Migné contaminated with NaCl according to procedure P1-1 W: (a) SEM image of the ground surface, (b) BSE image of the polished section.

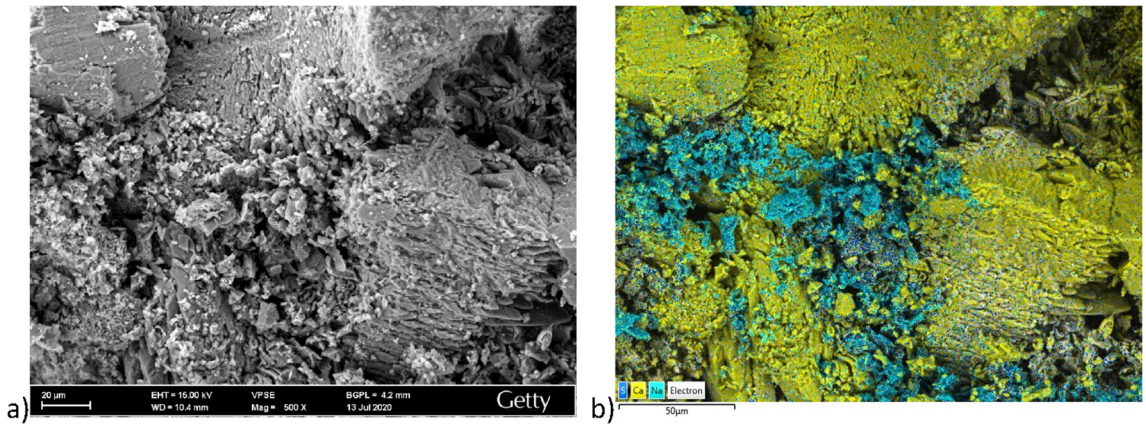


**Fig. 15.** SEM images of the fresh fracture close to the evaporative surface of Maastricht contaminated with $Na_2SO_4$ according to procedure P1-1S: (a) BSE image, (b) False colour image after EDS analysis, showing the distribution of calcium (yellow), sodium and sulphur (cyan and blue respectively). (For interpretation of the references to color in this figure legend, the reader is referred to the web version of this article.)

outer layer than stones contaminated with procedure **P2**. In the case of **$Na_2SO_4$**, **P2** induced a higher salt content in the outer layer of both stones.

Mass loss was negligible (lower than 0.05 wt%) in both materials contaminated with each procedure with **NaCl**. In the case of **$Na_2SO_4$**, slight damage occurred with procedures **P1-S** and **P2**. With procedure P1, rewetting caused severe damage in the case of the less porous stone **Migné** (**P1-1 W**) in the form of bursting, whereas Maastricht showed increasingly higher granular disintegration upon rewetting, leading to the conclusion that rewetting triggers damage propagation. The reason for the severe damage observed in **Migné** after rewetting (**P1-1 W**) is probably attributed to a high degree of pore filling after salt contamination (**P1-1S**) and to the development of high stresses in the small pores of this stone after dissolution/recrystallisation of the salt introduced. In the case of **Maastricht**, it can be assumed that the stress developed was not as high since the pores are larger and the resulting pore filling (also with ca. 1 wt% of salt introduced) is thus lower; consequently, the resulting damage was also less.

The salt types considered in this study follow long-term research studies and recommendations, as presented in the introductory section. The same salt content (1 wt% of the dry weight of the specimens) was used in all procedures to facilitate comparison. The accumulation procedures were tested in two stones with very similar composition but different porous structure to enable an easier and reliable comparison of the results (e.g., exclude differences in decay which could come from other damage processes, such as chemical reactions, hygric dilation, etc.). Besides, both stones have a unimodal pore size distribution, which simplifies further the comparison. Introducing a realistic salt content into the material and ensuring that the salt accumulates in a thin layer of the material close to the evaporative surface will lead to high salt pore filling. Hence, the damage propagation phase (entailing fast repeated wet-dry cycles) will trigger damage that reproduces onsite salt crystallisation mechanisms. The applicability of the most effective procedure (P1-1S) has been validated by D'Altri et al. [12], who reproduced the protocol by a multiphase numerical model. The numerical model confirmed the results obtained in the two limestones tested and indicated that the procedure is also valid for other types of porous building materials.

Pore clogging and the change of the surface properties due to efflorescence can affect the Stage II drying rate. The different transport properties between Migné and Maastricht, and the different salt solution concentrations used in each stone, are also likely to influence the salt distribution and the resulting pore clogging. Eloukabi et al. [41] studied the effect of NaCl on the drying of porous media. They found that a salt layer on the evaporative surface of a system with a large pore size does not significantly affect the

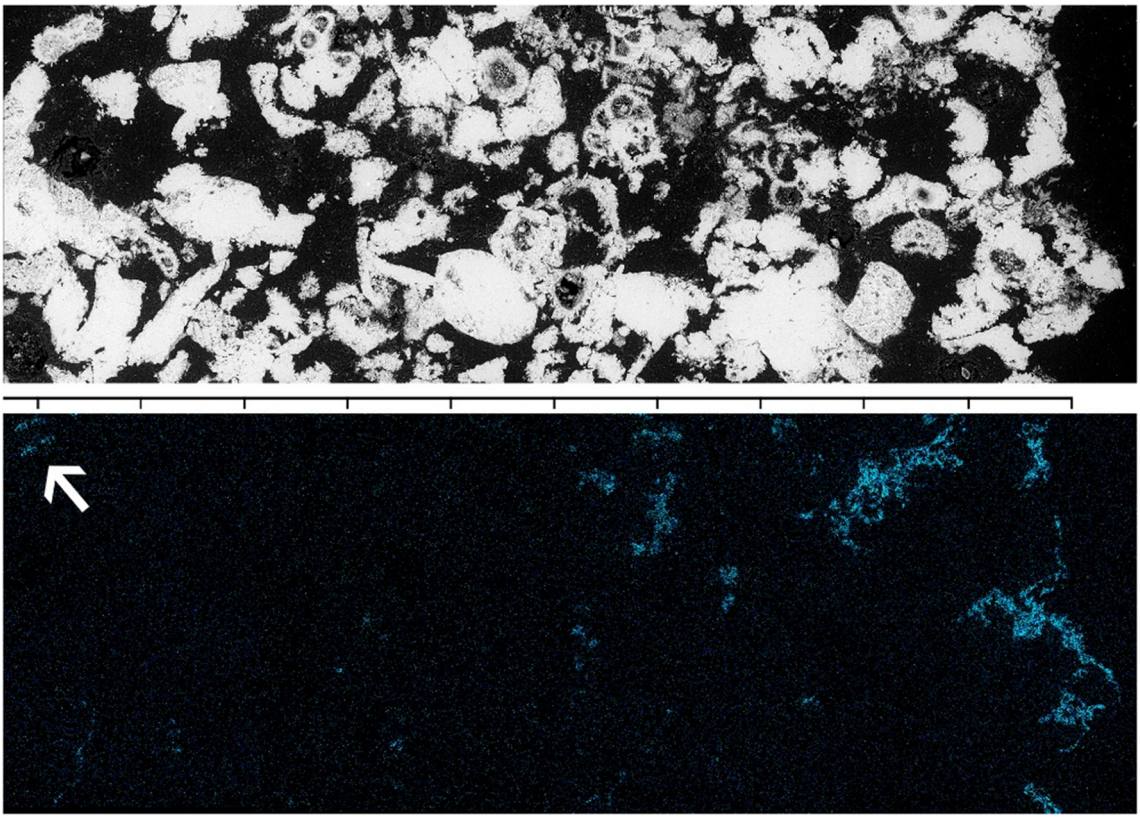

**Fig. 16.** Maastricht contaminated with $Na_2SO_4$ according to procedure P1-1S. In both images, the evaporative surface is located on the right side. Above: BSE image of the cross-section. Below (same cross-section): EDS false-color map showing the salt distribution according to depth (sodium and sulphur are shown in cyan and blue, respectively; contrast has been enhanced for better clarity) with the presence of salt clusters up to 2 mm depth (arrow). Scale segments = 200 μm. (For interpretation of the references to color in this figure legend, the reader is referred to the web version of this article.)

drying rate and can even accelerate it if the pore sizes are sufficiently large. In contrast, a NaCl layer formed on the evaporative surface of porous media with small pore sizes significantly limited the rate of evaporation. The authors assigned this phenomenon to the fact that, in large pore sized media, the NaCl efflorescence can grow upward, leading to patchy cauliflower efflorescence, as in the case of **Maastricht** contaminated with **NaCl** with procedure **P1-1S** (Fig. 4). In contrast, in the case of small pore size media, the salt crystals grow laterally rather than vertically, resulting in a salt crust that may block evaporation, as observed in **Migné** contaminated with **NaCl** with procedure **P1-1S** (Fig. 14). This hypothesis is also consistent with the results of the amount of salt efflorescence formed (Fig. 6); in general, in the case of **Migné**, there is lower salt efflorescence forming than in **Maastricht**, which indicates a higher amount of subflorescence, thus of pore clogging, hence affecting more severely the drying rate.

### *4.2. Comparison of methods for the analysis of the salt distribution*

The salt distribution in the specimens was one of the criteria guiding the choice of the accumulation procedure. Besides, the salt distribution through the depth of the specimen can provide useful information about the risk of damage in salt crystallisation tests: a higher salt accumulation in a thin layer of material close to the evaporative surface implies potentially higher crystallisation pressure and thus a higher risk of damage. Therefore, a reliable measurement of the salt content and distribution is crucial in salt crystallisation tests. In this study, several methods used for assessing the salt distribution have been tested; their advantages and disadvantages, resulting from past experience and from the present research, are summarized in Table 5 and described in detail hereafter.

**HMC** is a simple and reliable method for the semi-quantitative analysis of samples contaminated with a single salt and can be used as an alternative or complementary method for more expensive chemical analyses, like **IC**. However, care should be taken to monitor precisely the RH inside the climatic chamber because a difference of 1% at very high RH, such as 95% RH, can lead to significant differences in the HMC values, especially when dealing with high salt contents and very hygroscopic salts, such as NaCl. Hence, in the case of NaCl, using an RH of 80% may be advantageous.

**μ-XRF** maps allow for the precise distribution of the salt in a representative section of samples (in this study, the entire sample section was mapped). However, it is an expensive and time-consuming type of analysis. **SEM** allows the most precise observation of the salt distribution in the pores, including information about the preferential location of the salt (e.g., in coarse or finer pores), the crystallisation form (e.g., thenardite or mirabilite), and the salt crystallisation habit. The main drawbacks of using SEM lie with the sample size and its representativeness, and the disturbance of the sample during preparation.

The results of **DRMS** and **ST** measurements performed in Migné and Maastricht contaminated according to procedure P1 were generally in line with the IC, μ-XRF, and SEM results. This confirms that these two micro-destructive methods can be successfully used to assess the distribution of salts in stone in a reliable way. The DRMS may further be used in-situ, thus providing a useful tool for comparison of laboratory results with practice.

The **UPV** results were in agreement with the results obtained by other techniques in the case of Maastricht stone contaminated

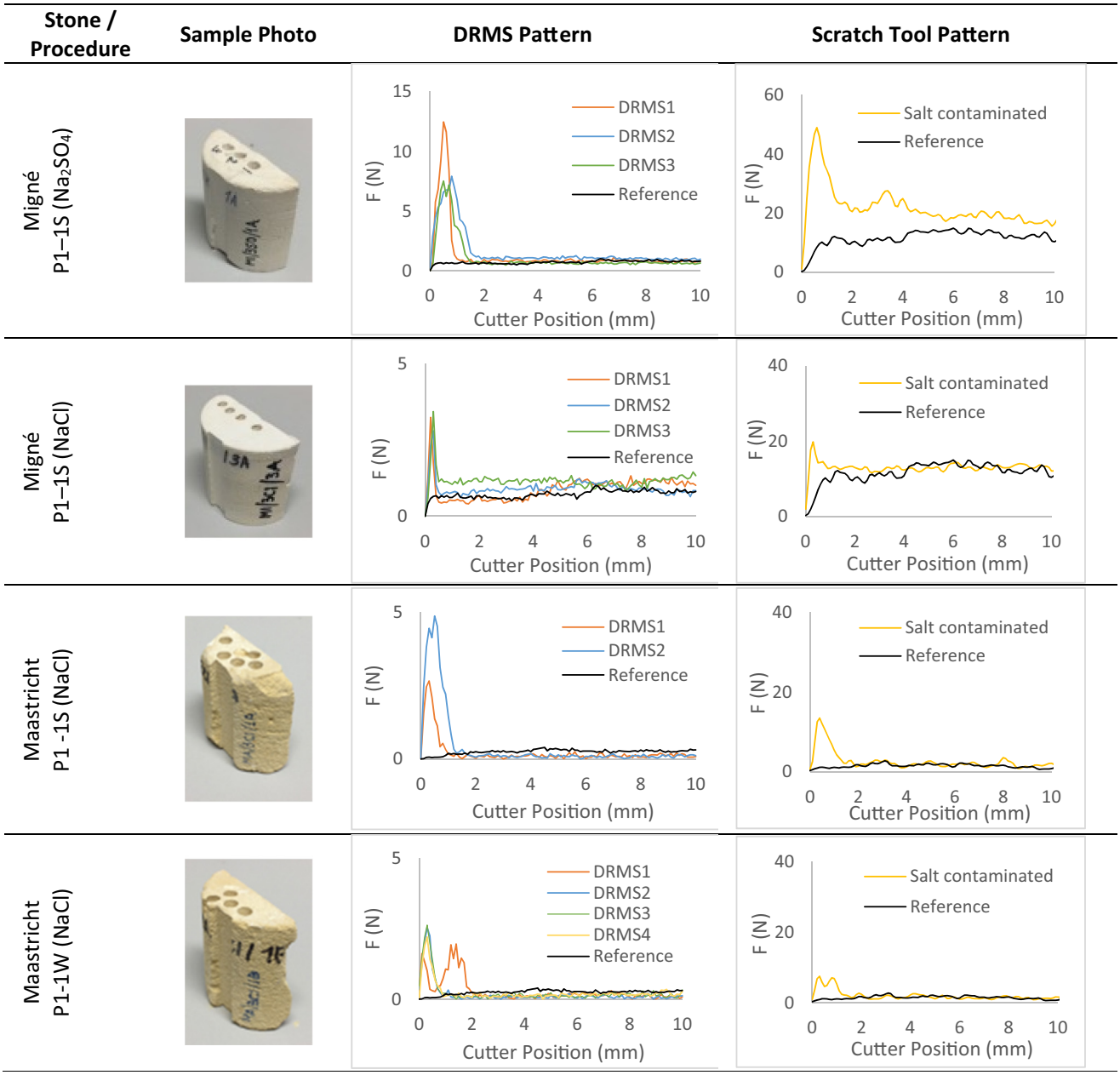


**Fig. 17.** DRMS and average ST patterns for samples contaminated according to procedure P1 (coloured lines) and reference samples (black lines).

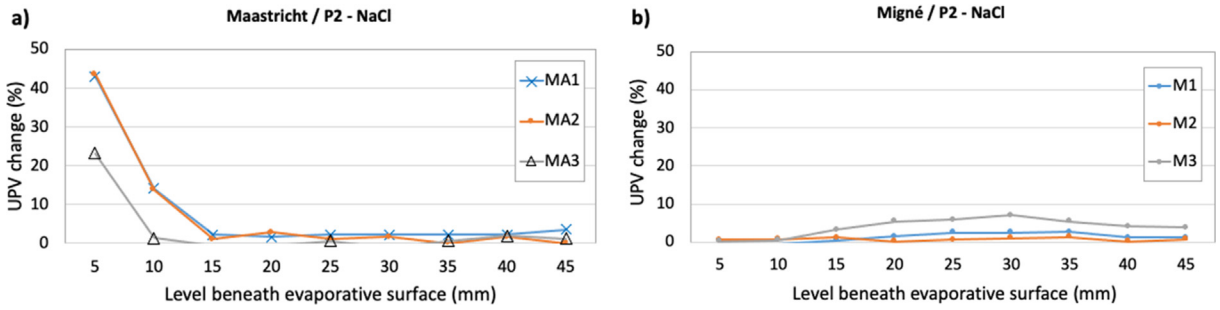


**Fig. 18.** UPV results registered in NaCl contaminated specimens with procedure P2 before and after salt contamination: (a) UPV changes in Maastricht stone measured at 5 mm intervals from the surface, (b) UPV changes in Migné stone measured at 5 mm intervals from the surface.

with NaCl. In contrast, in the case of Migné stone contaminated with NaCl, the UPV technique was not able to reveal the accumulation of salts in the outer layer, observed by the other investigation techniques. These results suggest that a higher number of

**Table 4**
Advantages and disadvantages of procedures P1 and P2 for accumulating salt in Migné and Maastricht stones.

| Procedure | Advantages | Disadvantages |
|---|---|---|
| P1-1S | - Accumulation of both salts in a thin layer of material (ca. 1 mm)- Low amount of salt efflorescence- Technically easy to perform in a reasonable time | - Can cause slight damage with $Na_2SO_4$ |
| P1-1 W & 2 W | - Rewetting once can promote further accumulation of NaCl in the outer layer of Migné | - Can cause medium to high damage with $Na_2SO_4$- Can cause redistribution of salt within the specimen thickness- Increases the amount of salt efflorescence- It is more time-consuming than P1-1S |
| P2 | - Higher salt enrichment in a thin layer of material (ca. 1 mm) with $Na_2SO_4$ | - Can cause medium damage with $Na_2SO_4$- Causes a higher amount of salt efflorescence than P1-1S- Is more time consuming than P1-1S |

**Table 5**
Advantages and disadvantages of each method of analysis used for assessing the salt distribution in Migné and Maastricht stones.

| Methods | Advantages | Disadvantages |
|---|---|---|
| IC | - Very high precision of ion quantity | - Expensive |
| HMC | - Technically simple- Enables the analysis of a large number of samples at the same time- Low cost | - Requires a climatic chamber- Time-consuming- May require further analysis to confirm the results |
| μ-XRF maps | - High precision of salt distribution in the entire sample section | - Expensive and time-consuming sample preparation |
| SEM | - Very high precision of salt distribution- Enables observing the morphology of the salt crystals and the region in which salt crystallizes preferentially | - Representativeness of sample (only small samples can be analysed)- Risk of disturbance of sample condition (salt distribution) during preparation |
| DRMS* & ST | - Good precision on homogeneous samples- Technically simple and fast- Micro-destructive | - DRMS requires performing several measurements for obtaining reliable results- Precision may be affected by the inhomogeneity of the material and the presence of hard minerals or vugs |
| UPV* | - Non-destructive | - Requires a suitable geometry of transducers (pointed shape)- Requires a large number of specimens for obtaining reliable results- Accuracy may depend on stone characteristic and salts |

* Can be performed in situ.

specimens should be considered for the UPV test to achieve more reliable results because its accuracy may depend on the stone and salt type; so, more tests are necessary to define the extent of the applicability of this method for detecting the salt distribution.

## 5. Conclusions

This study focused on the comparison of two contamination procedures for the accumulation of salts in two limestones, as well as on the comparison of different methods for the analysis of salt distribution.

Procedure P1-1S (capillary absorption of a salt solution followed by one drying cycle) proved to be the fastest and most effective in accumulating NaCl and $Na_2SO_4$ in a thin layer of material close to the evaporative surface, without resulting in too much salt efflorescence or damage in two types of stone with very different porous structure (Maastricht and Migné limestones). Hence, this procedure has been selected for reproduction using a multiphase numerical model [12]. The numerical model confirmed the obtained results in the tested limestones and indicated that the procedure is also valid for other types of porous building materials. Round robin tests with different types of porous building materials are currently ongoing to experimentally validate the test and to continue with the damage propagation phase.

All methods used in this study are considered useful for analysing salt distribution. Depending on the aim of the analyses, preferences exist. When non-destructive or minimally destructive techniques are to be preferred, DRMS, ST, and, with further improvement, UPV can offer a solution for the monitoring of salt distribution. If sampling is possible, HMC is a simple technique, not requiring specialized personnel, to obtain a reliable indication of the salt content and distribution. When more precise, quantitative information on the salt content is needed, IC is the most suitable technique. SEM and μ-XRF are most useful to provide information about the distribution of salts in pores, their specific location, and crystallisation form.

In general, a combination of screening measurements, carried out by simple and cheap techniques, such as HMC, DRMS, UPV, followed by further analysis on a selection of most relevant samples (chosen based on the results from the screening) with more sophisticated techniques, such as IC, SEM, and μ-XRF seems to be the most suitable and sustainable choice.

The future work of the TC ASC-271 will focus on the propagation phase. Round robin tests with other types of porous building materials are currently ongoing.

## CRediT authorship contribution statement

**Cristiana Nunes:** Data curation, Methodology, Writing - original draft. **Asel Maria Aguilar Sanchez:** Data curation, Methodology. **Sebastiaan Godts:** Data curation, Methodology. **Davide Gulotta:** Data curation, Methodology. **Ioannis Ioannou:** Data curation, Methodology. **Barbara Lubelli:** Methodology, Project administration, Writing - review & editing. **Beatriz Menendez:** Data curation, Methodology. **Noushine Shahidzadeh:** Data curation, Methodology. **Zuzana Slížková:** Data curation, Methodology. **Magdalini Theodoridou:** Methodology.

## Declaration of Competing Interest

The authors declare that they have no known competing financial interests or personal relationships that could have appeared to influence the work reported in this paper.

## Acknowledgements

All authors acknowledge Kévin Beck for providing the characterisation of the stones and Véronique Vergès-Belmin for providing the stone specimens used in this study. All authors also thank Rob Van Hees for a thorough reading and helpful comments on the paper. The authors are also thankful to all the other RILEM TC ASC-271 members for their contribution in discussions, especially

Tim De Kock and Julie Desarnaud, who have performed relevant experiments for future work.

Cristiana Nunes thanks Kateřina Mlsnová for helping with the specimens' preparation for the contamination procedures. Sebastiaan Godts acknowledges Mohamed Rich, Xavier Monfort, and graduate interns Simone Semprini, Elien Decaesteker, and Alice Vrancken for their help with sample preparation, IC, and HMC analysis. Ioannis Ioannou thanks RILEM member Loucas Kyriakou for his help with the ST and DRMS tests. Zuzana Slížková acknowledges Marek Eisler for performing the UPV analysis and the support from the Czech Academy of Sciences under the program "Strategy AV21-23. City as a Laboratory of Change; Construction, Historical Heritage and Place for Safety and Quality of Life."

Three anonymous reviewers provided valuable comments to improve the paper.

## References

[1] C. Alves, C. Figueiredo, J. Sanjurjo-Sánchez, Rock features and alteration of stone materials used for the built environment: a review of recent publications on ageing tests, Geosciences 10 (3) (2020) 91, https://doi.org/10.3390/geosciences10030091.

[2] B. Lubelli, V. Cnudde, T. Diaz-Goncalves, E. Franzoni, R.P. Van Hees, I. Ioannou, B. Menendez, C. Nunes, H. Siedel, M. Stefanidou, V. Verges-Belmin, H. Viles. Towards a more effective and reliable salt crystallisation test for porous building materials: state of the art, Mater. Struct. 51(2) 2018 10.1617/s11527-018-1180-5.

[3] CEN (1999) EN 12370 Natural stone test methods. Determination of resistance to salt crystallisation.

[4] RILEM, Recommended tests to measure the deterioration of stone and to assess the effectiveness of treatment methods, Test vol 1a—crystallisation test by total immersion (for untreated stone); Test V.1b—crystallisation test by total immersion (for treated stone); Test V.2— crystallisation test by partial immersion, Mater. Struct. 13 (75) (1980) 175–253.

[5] RILEM TC 127-MS (1998) MS-A.1— determination of the resistance of wallettes against sulphates and chlorides, Mater. Struct. 31:2–9.

[6] RILEM TC 127-MS (1998) MS-A.2— uni-directional salt crystallisation test for masonry units, Mater. Struct. 31:10–11.

[7] WTA Merkblatt 2-9-04/D (2005) Sanierputzsysteme/Renovation mortar systems. WTA Publications, Stuttgart.

[8] CEN (2003) EN 14147 Natural stone test methods - Determination of resistance to ageing by salt mist.

[9] ASTM B117-03 (2003) Standard Practice for Operating Salt Spray (Fog) Apparatus.

[10] K. Tuutti. Corrosion of steel in concrete. CBI Forsk. 824. http://lup.lub.lu.se/record/3173286 (accessed May, 2020) 1982.

[11] R. Flatt et al. Predicting salt damage in practice: a theoretical insight into laboratory tests, RILEM Technical Lett. 2 2017 108–118. 10.21809/rilemtechlett.2017.41.

[12] A.M. D'Altri, S. de Miranda, K. Beck, T. De Kock, H. Derluyn (submitted to publication in the Construction and Building Materials journal) towards a more effective and reliable salt crystallisation test for porous building materials. Part II: Predictive modelling of salt distribution.

[13] M. Angeli, D. Benavente, J.P. Bigas, B. Menendez, R. Hebert, C. David. Modification of the porous network by salt crystallisation in experimentally weathered sedimentary stones, Mater. Struct. 41(6) 2007 1091–1108. 10.1617/s11527-007-9308-z.

[14] K. Beck, M. Al-Mukhtar, Evaluation of the compatibility of building limestones from salt crystallisation experiments, Geol. Soc. Lond. Spec. Publ. 333 (1) (2010) 111–118, https://doi.org/10.1144/sp333.11.

[15] N. Shahidzadeh-Bonn, J. Desarnaud, F. Bertrand, X. Château, D. Bonn, Damage in Porous media due to salt crystallisation, Phys. Rev. E 81 (6) (2010), https://doi.org/10.1103/physreve.81.066110 066110.

[16] I. Ioannou, C. Hall, W.D. Hoff, V.A. Pugsley, S.D.M. Jacques. Synchrotron radiation energy-dispersive X-ray diffraction analysis of salt distribution in Lépine limestone, Analyst 130 2005 10.1039/b504274g.

[17] H. Derluyn, P. Vontobel, D. Mannes, D. Derome, E. Lehmann, J. Carmeliet, Saline water evaporation and crystallization-induced deformations in building stone: insights from high-resolution neutron radiography, Transp. Porous Media 128 (3) (2019) 895–913, https://doi.org/10.1007/s11242-018-1151-x.

[18] A.S. Goudie. Laboratory simulation of "the wick effect" in salt weathering of rock, Earth Surf. Proc. Land 11(3) 1986 275–285. 10.1002/esp.3290110305.

[19] C. Rodriguez-Navarro, E. Doehne, Salt weathering: influence of evaporation rate, supersaturation and crystallisation pattern, Earth Surf. Proc. Land. 24 (3) (1999), https://doi.org/10.1002/(sici)1096-9837(199903)24:3<191::aid-esp942>3.0.co;2-g.

[20] D. Benavente, M.A. García del Cura, A. Bernabéu, S. Ordóñez, Quantification of salt weathering in porous stones using an experimental continuous partial immersion method, Eng. Geol. 59 (3-4) (2001) 313–325.

[21] S. Modestou, I. Ioannou, Tracing the salt crystallisation front in limestone using the DRMS, in: E. Papamichos, P. Papanastasiou, E. Pasternak, A. Dyskin (Eds.), Bifurcation and degradation of geomaterials with engineering applications. Springer Series in Geomechanics and Geoengineering, 2017, https://doi.org/10.1007/978-3-319-56397-8_33.

[22] R. Nogueira, A.P. Ferreira Pinto, A. Gomes, Artificial ageing by salt crystallization: test protocol and salt distribution patterns in lime-based rendering mortars, J. Cultural Heritage 45 (2020) 180–192, https://doi.org/10.1016/j.culher.2020.01.013.

[23] P. Lopez-Arce, M. Tagnit-Hammou, B. Menendez, J.-D. Mertz, A. Kaci. Durability of stone-repair mortars used in historic buildings from Paris, Mater. Struct. 49 (12) 2016 5097–5115. 10.1617/s11527-016- 0846-0.

[24] C. Nunes, O. Skruzná, J. Válek. Study of nitrate contaminated samples from a historic building with the hygroscopic moisture content method: contribution of laboratory data to interpret results practical significance, J. Cult. Herit. 30 2018 57-69. 10.1016/j.culher.2017.09.013.

[25] B. Menendez, V. Petranova. Effect of mixed vs single brine composition on salt weathering in porous carbonate building stones for different environmental conditions, Eng. Geol. 210 2016 124–139. 10.1016/j.enggeo. 2016.06.011.

[26] C. Cardell, D. Benavente, J. Rodríguez-Gordillo, Weathering of limestone building material by mixed sulfate solutions. Characterization of stone microstructure, reaction products and decay forms, Mater. Charact. 59 (10) (2008) 1371–1385, https://doi.org/10.1016/j.matchar.2007.12.003.

[27] E. Ruiz-Agudo, F. Mees, P. Jacobs, C. Rodriguez-Navarro, The role of saline solution properties on porous limestone salt weathering by magnesium and sodium sulfates, Environ. Geol. 52 (2) (2007) 269–281.

[28] K. MacWilliam, C. Nunes, Towards a more realistic and effective use of sodium sulfate in accelerated ageing of natural stone, Struct. Anal. Historic. Constr. 1949–1958 (2019), https://doi.org/10.1007/978-3-319-99441-3_209.

[29] S. Godts, R. Hayen, H. De Clercq, Common salt mixtures database: a tool to identify research needs, in: De Clercq (Ed.), Proc, KIK-IRPA, Brussels, 2014, pp. 185–198.

[30] D. Benavente, M.A. García del Cura, R. Fort, S. Ordóñez, Durability estimation of porous building stones from pore structure and strength, Eng. Geol. 74 (1-2) (2004) 113–127, https://doi.org/10.1016/j.enggeo.2004.03.005.

[31] J. Desarnaud, F. Bertrand, N. Shahidzadeh-Bonn, Impact of the kinetics of salt crystallisation on stone damage during rewetting/drying and humidity cycling, J. Appl. Mech. 80 (2) (2013), https://doi.org/10.1115/1.4007924.

[32] P.M. Benson, P.G. Meredith, E.S. Platzman, R.E. White, Pore fabric shape anisotropy in porous sandstones and its relation to elastic wave velocity and permeability anisotropy under hydrostatic pressure, Int. J. Rock Mech. Min. Sci. 42 (2005) 890–899, https://doi.org/10.1016/j.ijrmms.2005.05.003.

[33] N. Aly, A. Hamed, M. Gomez-Heras, D. Benavente, M. Alvarez de Buergo. The Effect of Salt Crystallisation on the Mechanical Properties of Limestone: Statistical Correlation between Non-destructive and Destructive Techniques, in Hughes JJ and Howind T (Eds.), Proc. 13th Int. Cong. on the Deterioration and Conservation of Stone, Paisley: University of the West of Scotland, 225-231 2016.

[34] S. Modestou, M. Theodoridou, I. Ioannou, Micro-destructive mapping of the salt crystallisation front in limestone, Eng. Geol. 193 (2015) 337–347, https://doi.org/10.1016/j.enggeo.2015.05.008.

[35] M. Theodoridou, F. Dagrain, I. Ioannou, Micro-destructive cutting techniques for the characterization of natural limestone, Int. J. Rock Mech. Min. Sci. 76 (2015) 98–103, https://doi.org/10.1016/j.ijrmms.2015.02.012.

[36] T. Diaz Goncalves, J. Delgado Rodrigues, Evaluating the salt content of salt-contaminated samples on the basis of their hygroscopic behaviour, Part I: fundamentals, scope and accuracy of the method, J. Cult. Herit. 7 (2006) 79–84, https://doi.org/10.1016/j.culher.2006.02.009.

[37] M. Nasraoui, W. Nowik, B. Lubelli, A comparative study of hygroscopic moisture content, electrical conductivity and ion chromatography for salt assessment in plasters of historical buildings, Constr. Build. Mater. 23 (5) (2009) 1731–1735, https://doi.org/10.1016/j.conbuildmat.2008.09.029.

[38] C. Price (Ed.), An expert chemical model for determining the environmental conditions needed to prevent salt damage in porous materials, European Commission Research Report No 11, (Protection and Conservation of European Cultural Heritage), Archetype Publications, London, 2000.

[39] ICOMOS-ISCS (2008) Illustrated glossary on stone deterioration patterns. Ateliers 30 Impression, Champigny/Marne.

[40] Monument Diagnosis and Conservation System. https://mdcs.monumentenkennis.nl/ (accessed May 2020).

[41] H. Eloukabi, N. Sghaier, S. Ben Nasrallah, M. Prat, Experimental study of the effect of sodium chloride on drying of porous media: the crusty–patchy efflorescence transition, Int. J. Heat Mass Transf. 56 (1-2) (2013) 80–93, https://doi.org/10.1016/j.ijheatmasstransfer.2012.09.045.